sciendo

Slovak Journal of Civil Engineering

Vol. 30, 2022, No. 3, 1 – 8
DOI: 10.2478/sjce-2022-0015

ANALYSIS OF STATIC AND CYCLIC TRAFFIC LOADING OF AN EMBANKMENT SUPPORTED BY A GEOGRID RETAINING STRUCTURE

Jakub, STACHO[1*], Monika, SULOVSKA[1]

Abstract

The article deals with a deformation analysis of a road embankment under different types of static and cyclic loading. A typical cross-section of a road embankment supported by geogrid retaining structures is considered. In the case of a design, the load is usually applied as a distributed static load. The analysis presented in the paper includes all the most loading methods used. Because there are only a few measurements for these types of construction in a given region, the analysis also includes a cyclic loading that aims to simulate real traffic loading. The cyclic loading considered the weights of cars and trucks and the distances between them, based on traffic intensity measurements. The study results showed how significant the differences in vertical and horizontal deformations of an embankment are when the different types and methods of static loading are used in a design. The results of the cyclic loading showed the deformations that can be expected from current real traffic.

Address

[1] Dept. of Geotechnics, Faculty of Civil Engineering, Slovak University of Technology in Bratislava, Bratislava, Slovakia

* ***Corresponding author:*** jakub.stacho@stuba.sk

Key words

- Traffic loading,
- Static loading,
- Cyclic loading,
- Road embankment,
- Geogrid retaining structure.

1 INTRODUCTION

The design of a road embankment supported by a geogrid retaining structure (GRS) is a type of construction increasingly used for expanding road infrastructures in Slovakia. In suitable conditions, the design of a road embankment supported by a GRS can lead to more effective, economical, and less time-consuming alternative to conventional methods. The typical applications of these types of constructions in Slovakia are discussed in, e.g., Dolinajova and Snahnican (2015); Adamec and Snahnican (2016); Silber-Hasslacher and Snahnican (2019); and Sulovska and Stacho (2019). The study presented in this article focuses on road embankments supported by a wrapped GRS with a passive facing system. In the case of a wrapped GRS, the geogrid is on the side of the face returned back into the soil/embankment, see, e.g., Scotland et al. (2014). In the case of a passive facing system, the wrapped GRS is built to a total height in the first step; then, an independent facing system is constructed and given the final form of the structure, see, e.g., Silber-Hasslacher and Snahnican (2019). The analysis presented is focused on vertical and horizontal deformations of an embankment supported by a GRS. The simple analytical and semi-empirical methods for determining the deformations of these structures have been presented by, e.g., Wu (1994) and Holtz and Lee (2002). The numerical modelling, which is based on the finite element method (FEM) or the distinct element method (DEM), was presented by, e.g., Scotland et al. (2016); Drusa and Vlcek (2016); and Wang et al. (2014). The modeling of any traffic loading on an embankment is a separate problem. A traffic load is mostly applied according to Eurocode 1: Actions on structures, Part 2: Traffic loads on bridges (EN 1991-2). Loading Model 1 (LM1) is used. The LM1 defines the magnitude of the loads for the individual loading lanes in a tandem system (TS) and a uniformly distributed load (UDL). According to this standard, the load from a TS and ULD can be distributed to an equivalent distributed load. This method is usually used in the case of the design of a construction supported by GRS. The load is applied as a design static load and represents the most critical situation during the life of a construction. It is used in different verifications of the ultimate limit state (ULS); however,

© 2022 The Author(s). This is an open access article licensed under the Creative Commons Attribution 4.0 License (https://creativecommons.org/licenses/by/4.0/).

the traffic load is not applied in verifications of the serviceability limit state (SLS). When the static load according to LM1 is used, the deformation of the embankment seems to be too great. The real traffic loading is variable, acts dynamically, and has a smaller magnitude, which means that real deformations of the embankment are significantly smaller. There is not enough permanent monitoring of the deformations of an embankment supported by GRS in Slovakia. For this reason, cyclic loading, the aim of which is to simulate a typical real traffic loading, was modelled. The magnitude of the loads and loading frequency were determined according to the traffic intensity measurements in the given road section.

2 CREATING THE NUMERICAL MODEL FOR THE CASE STUDY

The numerical model of the embankment supported by GRS was done using the Plaxis geotechnical software. The calculations are based on FEM. This software permits modeling a construction process and executes a detailed deformation analysis of an embankment and subsoil under different types of loads. The scheme of the model focused on an embankment supported by GRS is shown in Fig. 1. The embankment has a height of 5.2 to 5.96 m above the terrain level. The width of the embankment at the top was 13.5 m. The whole dimensions of the model were 70 x 30 m, which was appropriate for the type of task. The model was created as a plane strain model using triangular 6-node elements, which were required to reduce the calculation time for the analysis of the cyclic loading. The mesh of the finite elements was refined especially close to the facing of the wrapped GRS to obtain its adequate horizontal deformation of the embankment. A view of the connectivity plot, the finite element mesh, is shown in Fig. 2. The soils were modelled using the Hardening small-strain (HSs) model, see Benz (2007). This constitutive model extends the "classic" Hardening soil (HS) model and permitts taking into account the very small-strain soil stiffness and its non-linear dependency on the strain amplitude. The parameters describing the deformation behavior of the soil are as follows: E_{50}^{ref} - secant stiffness in a standard drained triaxial test; E_{oed}^{ref} - tangent stiffness for the primary oedometer loading; E_{ur}^{ref} - unloading/reloading stiffness; m - power for the stress-level dependency of the stiffness; G_0^{ref} - the initial small-strain shear modulus; and $g_{0.7}$ - the shear strain level of the secant shear modulus. G_s is reduced to about 70% of G_0. The subsoil was modelled as A-type undrained, and the material of the embankment was modelled as drained, see, e.g., the Plaxis manual (2021). The basic properties used in the model are stated in Tab. 1, where γ is the unit weight, g_{sat} is the saturated unit weight; j' is the drained angle of the shear strength; y' is the angle of the dilation, and c' is the drained cohesion. Based on the engineering-geological survey, the subsoil consists of clayey sand. The body of the embankment was designed from silty gravel. The properties, such as γ, g_{sat}, j', c', and E_{oed} were determined according to, e.g., Sulovska and Stacho (2019). In this study, it was assumed that $E_{50}^{ref} = E_{oed}^{ref}$, and $E_{ur}^{ref} = 4 . E_{oed}^{ref}$ in the case of the clayey sand and $E_{ur}^{ref} = 3 . E_{oed}^{ref}$ in the case of the gravels. The angle of the dilatancy of the gravel was determined as $y' = j' - 30°$, see e.g., PLAXIS 2D CE V21.01:1 (2021). Other parameters required for the HSs material model, such as $g_{0.7}$ and G_0^{ref}, were determined according to recommendations made by Ladicsova (2017).

The compacted gravel between the facing blocks and wrapped main body of the embankment, gravel bed, and base course, are usually created of compacted poorly graded gravel. Although the grain size of the material may vary in the backfill, gravel bed, and base course, the same relatively conservative properties are usually used in a practical design, see, e.g., Sulovska and Stacho (2019). Gravel properties, i.e., silty gravel as well as poorly graded gravel, were determined according to STN 72 1001: Classification of soil and rock.

The foundation strips, facing blocks, and asphalt pavement were modelled using only the standard Linear elastic (LE) material model, which adequately simulates the behaviour of these elements. The concrete had the following properties: Young's modulus, E = 35 GPa, and Poisson's ratio, v = 0.2. The wearing course of the pavement had the following properties: an axial stiffness $E.A$ = 97.8 MN.m^{-1}; a bending stiffness $E.I$ = 326 MN.m^{-2}.m^{-1}; and v = 0.35. The geogrid was modelled using an elastoplastic, isotropic geogrid type of material. The elastic stiffness $E_{geogrid}.A_{geogrid}$ was defined at a value of 1100 kN.m^{-1}, and the plastic threshold N_p was applied at a value of 80 kN.m^{-1}. The property of the interface between the geogrid and soil is given by the R_{inter} parameter. The R_{inter} was assumed

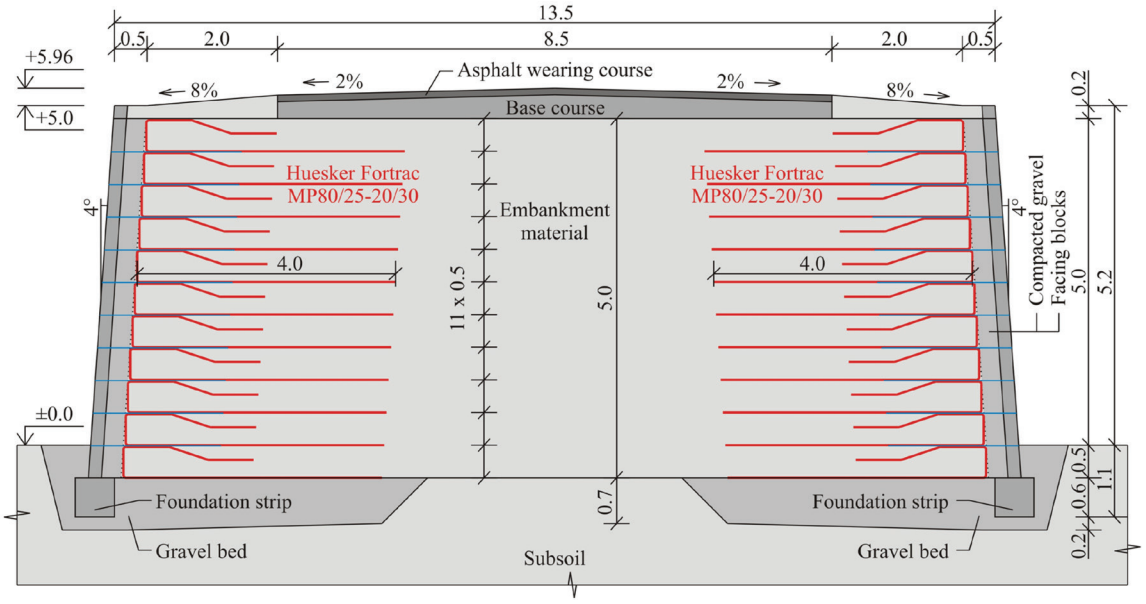


Fig. 1 *Scheme of the road embankment supported by GRS*

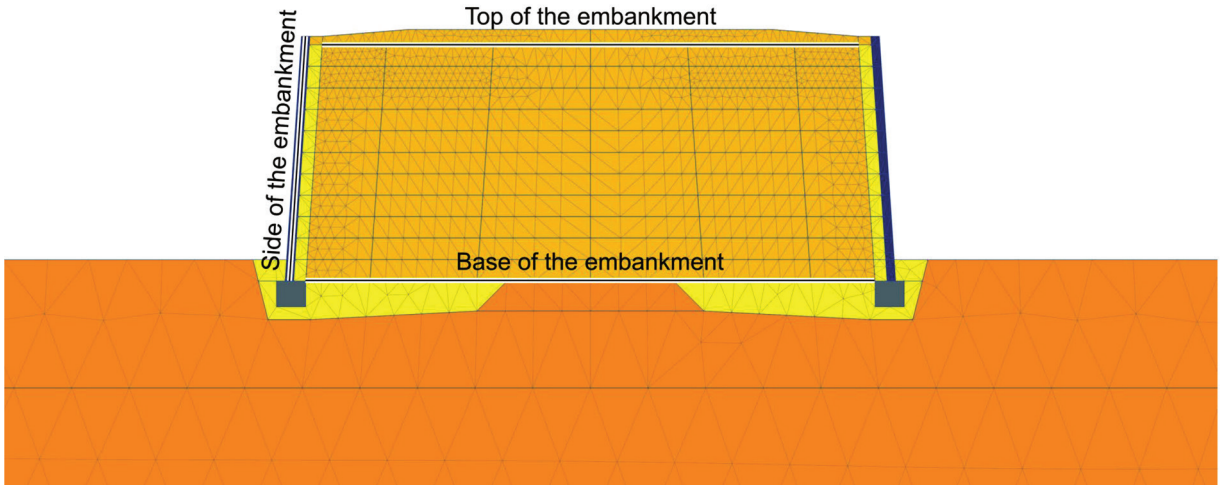


Fig. 2 *Detail of the finite element mesh of the embankment*

at a value of 1.0, which was determined from the study results presented by Stacho et al. (2020). The same consideration was given by Mirmoradi and Ehrlich (2015). The connection between the two geogrids was modeled as rigid. The active length of the geogrid was 4.0 m. The placing of the geogrids is also shown in Fig. 1.

Tab. 1 *Properties of the soils used in the calculations*

Parameter	Unit	Material / Soil		
		Embankment (Silty gravel)	Poorly graded gravel	Subsoil (Clayey sand)
γ	(kN.m^{-3})	19	19	20.3
g_{sat}	(kN.m^{-3})	19	19	20.3
E_{50}	(MN.m^{-2})	84	95	11.7
E_{oed}	(MN.m^{-2})	84	95	11.7
E_{ur}	(MN.m^{-2})	252	285	46.8
m	(-)	0.5	0.5	0.7
G_0	(MN.m^{-2})	157.5	178.0	60.84
$g_{0,7}$	(-)	0.0002	0.0002	0.0003
j'	(°)	28	35	24
y'	(-)	0	5	0
c'	(kN.m^{-2})	5	0	12
Drainage Type	(-)	Drained	Drained	Undrained A

The process of the construction of the embankment supported by GRS was modelled in 19 phases. The phases were modelled as consolidation phases, and the time of each stage was given according to the real construction time of a similar embankment on the same motorway. The initial phases were focused on the landscaping and the construction of the concrete foundation strips. Subsequently, the wrapped body of the embankment was constructed step by step to its full height. The construction of the wrapped GRS was simulated according to a layer-by-layer formwork method. In this part of the calculations, the pure wrapped embankment had relatively significant deformations. After the complete consolidation phase, the deformations were set to zero, and the construction of the facing system and road construction was modelled. The facing blocks were placed 0.3 m from the wrapped GRS body. The space between them was filled by compacted gravel. The facing blocks were connected with the wrapped GRS using the activation of the connecting geogrids. Subsequently, the construction of the road was modelled. The complete consolidation phase ended the modelling of the construction of the embankment. This numerical model was later used in the analysis, where different static and cyclic load types were applied.

2.1 Determining the load from the traffic

In the first part of the analysis, the static load was applied in the numerical modelling. The traffic load was used according to Eurocode 1: Actions on structures, Part 2: Traffic loads on bridges (EN 1991-2). The loads for the individual lanes in the form of TS (acting as the point load) and UDL (acting as the distributed load) were applied according to LM1; see Tab. 2. According to this standard, the load from TS and ULD could be distributed to an equivalent distributed load.

Tab. 2 *Application of the load according to LM1 of the EN 1991-2 standard*

Loading type		Width of the lane	TS	UDL	Coefficients for the road category	
Marking (Unit)		(m)	$Q_{i,k}$ (kN)	$q_{i,k}$ (kN.m^{-2})	$a_{Q,i}$ (-)	$a_{q,i}$ (-)
Location	Lane No.1	3	300	9	0.9	0.9
	Lane No.2	3	200	2.5	0.9	1
	Lane No.3	3	100	2.5	0.9	1
	Remaining area	-	-	2.5	-	1

According to the standard, the loading lanes must be placed to achieve the most critical situation for the design; however, it is not exactly clear how the load must be applied in the given type of construction when the different conditions require placing the load in various positions. For this reason, two options are used in the practical design. The first option considers placing Lane No.1 on both sides of the road and the remaining area between them, see *Loading model A* (Fig. 3). The second option considers the loading on one side, i.e., Lanes Nos. 1 and 2, and the remaining area on the other side of the road, see *Loading model B* (Fig. 3). In the case of *Loading model A* (Fig. 3), two schemes were used, i.e., *Scheme 1*, where all the loads were distributed to a single load f_k, and *Scheme 2*, where the loads in the loading lanes were distributed to load $f_{k,1}$, while the load in the remaining area $q_{2,k}$ corresponds to $f_{2,k}$. In *Loading model B*, the loads in the loading lanes and the remaining lanes are directly distributed to loads $f_{1,k}$; $f_{2,k}$; and $f_{3,k}$ (Fig. 3). The EN 1991-2 standard recommends a load distribution from TS to an area of 6.6 m^2. This option can lead to determining relatively significant deformations, which are often assumed to be unreal. For this reason, the load from TS is distributed to an area of 15 m^2 in the practical design. Both options were used in the study presented in this paper. The characteristic distributed loads for each scheme are summarized in Tab. 3.

In the second part of the analysis, the load was modelled as cyclic and simulated the real traffic load. The numerical modelling of cyclic loading can be done in different ways. An analysis of an embankment or platform under dynamic/cyclic and cyclic loading has been presented by, e.g., Abdelkrim et al. (2003); Zheng et al. (2012); Xuecheng et al. (2010); and Zhuang and Li (2015). In the case of a dynamic analysis, the common problem in numerical modelling is the time required for the calculations and the heavy demands on a computer's hardware. Adam et al. (2000) presented a 3D modelling approach performed with a coupled boundary element-boundary element method and a 2D modelling approach performed by a coupled boundary element-finite element method. They demonstrated effective algorithms for reducing the time and system requirements for the calculations. Another important aspect of the modeling is the way in which the dynamic/cyclic load is defined. In most analyses, the load is specified using a traditional sinusoidal course, see, e.g., Zhuang and Li 2015; Han et al. 2015; Pham and Dias (2019). Other ways of modelling the cyclic load have been presented by, e.g., Zheng et al. (2012), who used a semisine course, or Abdelkrim et al. (2003) and Liu et al. (2017), who demonstrated a simulation of a moving strip or point load, respectively.

Tab. 3 *Loads applied in the numerical modeling in the different models*

Loading type	Loading scheme	Model	Characteristic distributed load		
			$f_{1,k}$	$f_{2,k}$	$f_{3,k}$
Static	Scheme 1	Model S1	31.9	-	-
		Model S2	64.21	-	-
	Scheme 2	Model S1	44.1	2.5	-
		Model S2	89.92	2.5	-
	Scheme 3	Model S1	44.1	26.5	2.5
		Model S2	89.92	57.04	2.5
Cyclic	Scheme 4	Model D1	*changing (Fig. 4)	-	-

In the case of the analyzed embankment supported by GRS, the real traffic intensity was considered. The traffic intensity measurements in the given road section showed that five small passenger cars and one truck passed through the section of the road in one minute. The average weight of the passenger cars at a value of 2.5 t was taken into account. In the case of the truck, the weight of the whole truck of 44.0 t was assumed (Fig. 4). The load was modelled as a distributed load acting as a step (jump) load for loading the road only for the time required to pass a car or truck, respectively, when the nominal speed of 90 km.h^{-1} is taken into account. These times and the times between the cars or between the cars and the truck are stated in Fig. 4. In this way, one loading cycle, which was repeated in numerical simulations, was defined. In this case, the real situation was modelled; as a result, the distributed load of the average width of 2.5 m was modelled in the middle of each lane, see *Loading Model C* and corresponding *Scheme 4* in Fig. 3.

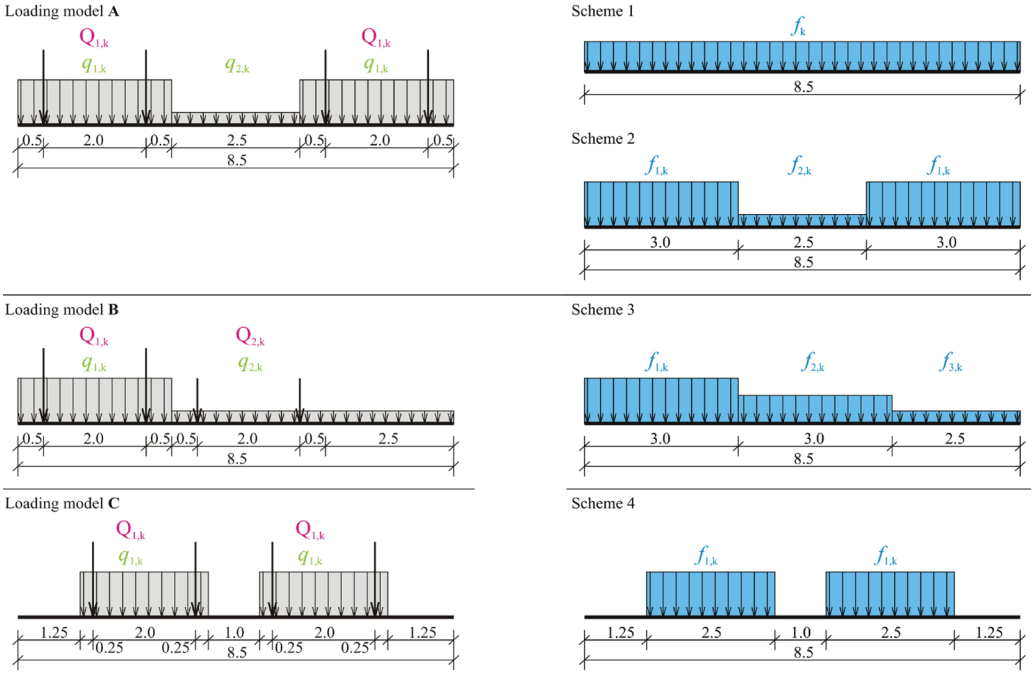


Fig. 3 *Schemes of the loading models and load distributions applied in the numerical modeling*

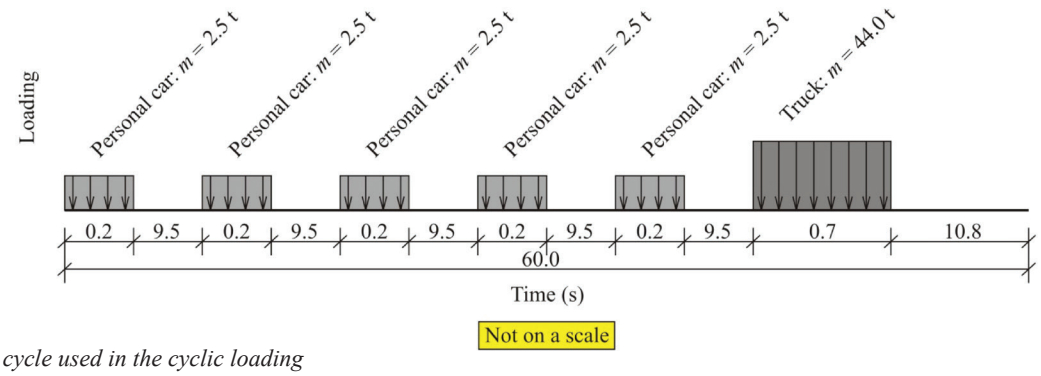


Fig. 4 *One-load cycle used in the cyclic loading*

3 THE RESULTS OBTAINED IN THE STUDY

The results of the study focus on a comparison of the vertical deformations on the top and bottom of the embankment, the horizontal deformations of the side of the embankment, and the passive facing system of the embankment, respectively, see Fig. 2. The total deformations are presented in Fig. 5 for the bottom of the embankment, Fig. 6 for the top of the embankment, and Fig. 7 for the side of the embankment. The first model marked *Initial stage - No traffic load*, represents a situation when no traffic load is applied on the embankment. The deformations are caused only by the construction of the top of the embankment and the construction of the road, respectively, and the construction of the passive facing system. Subsequently, combinations of the different static loads applied were assembled. The application of the loading in *Schemes 1*, *2*, and *3*, is shown in Fig. 3. *Model S1* takes the distribution of the load from TS to an area of 15 m^2 into account, and *Model S2* takes the distribution of the load from TS to an area of 6.6 m^2 into account. The following combinations of models and loading were assembled:

- *Model S1 - Scheme 1*,
- *Model S1 - Scheme 2*,
- *Model S1 - Scheme 3*,
- *Model S2 - Scheme 1*,
- *Model S2 - Scheme 2*,
- *Model S2 - Scheme 3*,

The results are presented for a situation when the static load acted on the embankment for the time required for complete consolidation. This permitted determining the final permanent deformation of the embankment, which was loaded by a different type of static loading. The results obtained for the cyclic loading are marked *Model D1 - Scheme 4*. In this case, the cyclic load was applied according to *Scheme 4* of *Loading model C*. The greatest permanent deformation of the embankment was achieved after 324 loading cycles. The results of the deformation of the embankment under cyclic loading are stated in section 3.1 in more detail.

The results showed that the vertical deformations determined in *Model D1 - Scheme 4* are slightly greater than those reached in the *Initial stage*. The difference is about 3 mm at the bottom of the embankment and about 11.5 mm at the top of the embankment. In *Model D1 - Scheme 4*, the horizontal deformation increased from 6.1 mm (Initial stage) to about 11.0 mm. These results showed that small deformations of the embankment only occur when simulating the actual traffic loading. Applying the static loading typically used in the design led to determining significantly greater embankment deformations. In *Model S1*, the vertical deformations of the top and bottom of the embankment are similar for all the loading schemes applied, except for the lesser loading side of the embankment in

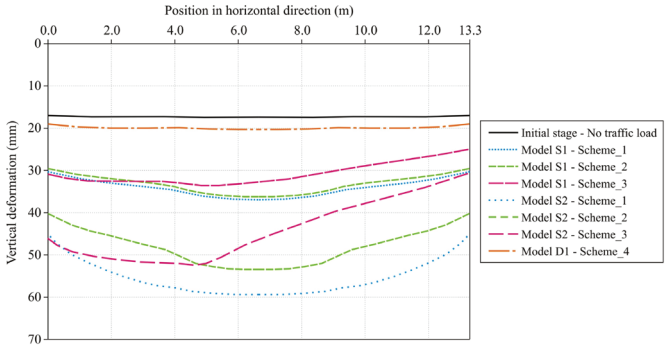


Fig. 5 *Vertical deformation of the base of the embankment*

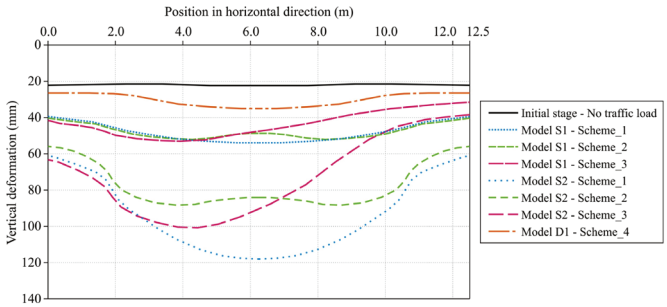


Fig. 6 *Vertical deformation of the top of the embankment*

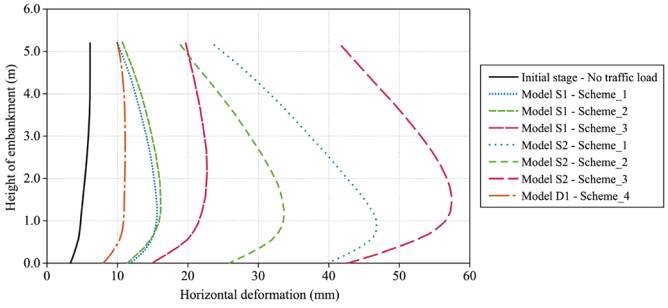


Fig. 7 *Horizontal deformation of the embankment*

Scheme 3. The vertical deformation of the bottom of the embankment was about 33 - 37 mm, and the vertical deformation of the top of the embankment was about 53 - 54 mm. The horizontal deformation of the embankment was about 15 mm in the case of *Model S1 - Scheme 1* and about 16 mm in the case of *Model S1 - Scheme 2*. In the case of *Model S1 - Scheme 3*, the horizontal deformation achieved was about 22.7 mm. In all three cases, the distribution area of 15 m^2 was applied to the TS. When the distribution area of 6.6 m^2 was used on the TS (*Model S2*), significantly greater vertical and horizontal deformations were achieved. The greatest vertical deformations of the top and the bottom of the embankment were

achieved when the load was applied according to *Scheme 1*; however, in the case of the horizontal deformations, the greatest value was achieved when the load is applied according to *Scheme 3*.

3.1 Deformation of the embankment under cyclic loading

The cyclic loading was applied according to the scheme in Fig. 4, which tries to simulate real traffic loading according to actual traffic intensity measurements. The loads were defined according to *Scheme 4* of *Loading model C* (Fig. 3). The vertical deformations of the top and bottom of the embankment over time are presented for the initial 180 cycles in Figs. 8 and 9, respectively. A significant increase in the deformations was achieved in the initial cycles; then, the incremental displacement was reduced over time. After 324 cycles, the stable value of the deformations was achieved. It was assumed that the stable value of the deformations was achieved when the excess pore pressure decreased below 1 kPa. The change in the maximum pore pressure over time for the initial 180 cycles is shown in Fig. 10.

The vertical deformations of the top and bottom of the embankment and the horizontal deformation of the side of the embankment, which is reached after 10, 100, and 324 cycles, are shown in Figs. 11, 12, and 13. The results presented also include the deformations determined in the initial stage. In the case of cyclic loading, the deformations increase significantly in the initial cycles, but this increase decreases over time or on the number of cycles, respectively.

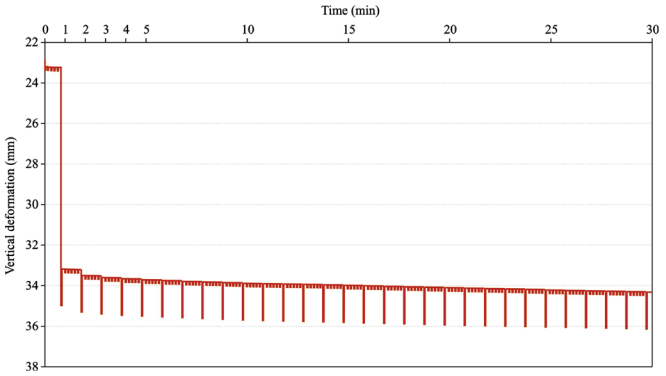


Fig. 8 *Vertical deformation of the top of the embankment over time - initial 180 cycles*

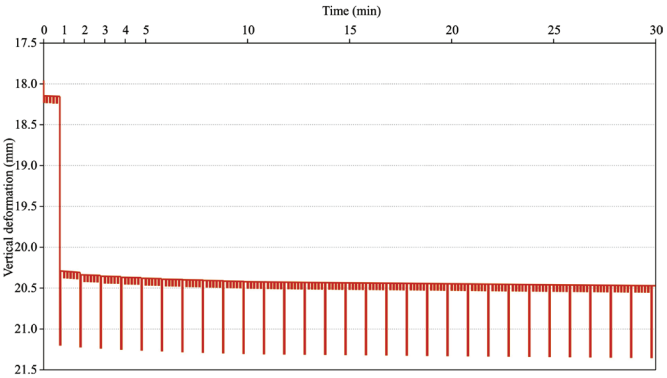


Fig. 9 *Vertical deformation of the base of the embankment over time - initial 180 cycles*

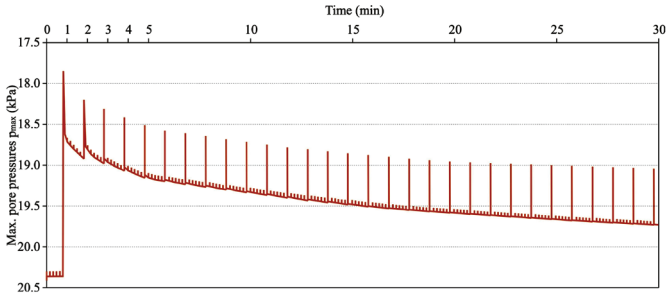


Fig. 10 *Course of the maximum pore pressure over time - initial 180 cycles*

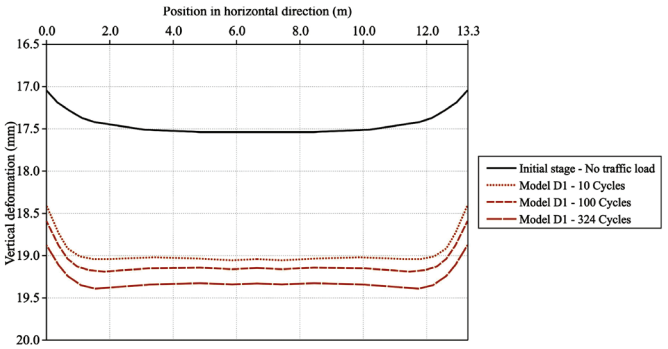


Fig. 11 *Vertical deformation of the base of the embankment in the case of cyclic loading*

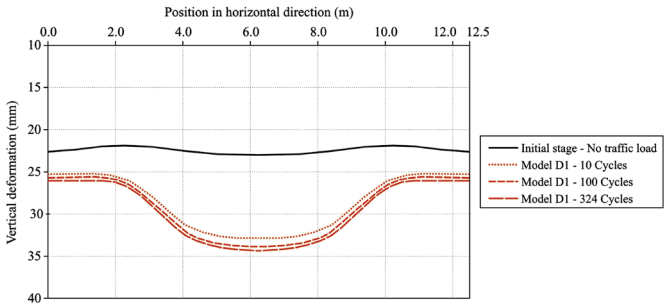


Fig. 12 *Vertical deformation of the top of the embankment in the case of cyclic loading*

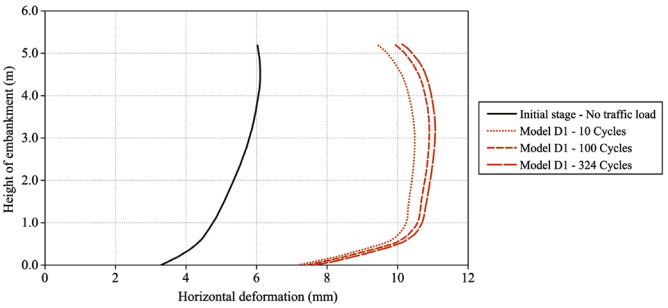


Fig. 13 *Horizontal deformation of the embankment in the case of cyclic loading*

The results more or less confirm that the deformations of the embankment are mainly caused by truck traffic. In the analysis presented, the subsoil of the embankment is relatively stiff and permeable. Based on the average traffic intensity, only one truck passes through the road section per minute. All these parameters lead to a relatively small number of cycles required to achieve a stable deformation. In the clayey subsoil, which requires a longer consolidation time and a greater intensity of truck traffic, the time and number of cycles needed to achieve a stable deformation can be significantly longer. The results also showed that in the case of the embankment design supported by GRS, the simulation of the cyclic loading permitted obtaining a magnitude of the estimated deformations that could occur under expected or design traffic loading.

4 CONCLUSIONS

The design of a road embankment supported by a geogrid retaining structure (GRS) with a passive facing system is based on verifications of the ultimate and serviceability limit states. The verification of the deformations of the embankment, as part of the serviceability limit state verifications, usually does not consider the acting variable traffic load. The visual monitoring of such constructions shows that some deformations from a traffic load occurs; however, the permanent monitoring for a given type of construction in the given region is missing. The results of the deformation analysis of the embankment supported by GRS under different types of loading showed that the type of loading and scheme have a significant impact on the deformations achieved. Different schemes based on the Load Model 1 of the EN 1991-2 standard were applied in the case of the static loading. If the load distribution from a tandem system (TS) to an area of 15 m^2 (which is often used in the practical design of given types of constructions) is applied, the vertical deformations of the top and bottom of the embankment are similar for all the loading schemes applied. In the horizontal deformations, the loading according to Scheme 3 led to determining the greatest horizontal deformations. If the load distribution from TS to an area of 6.6 m^2 is applied, according to the recommendations of the standard, the vertical and horizontal deformations of the embankment are significantly greater. The greatest vertical deformations of the embankment were achieved when the load was applied according to Scheme 1, and the greatest horizontal deformations were achieved when the load was used according to Scheme 3. The cyclic loading simulated the real traffic loading determined according to the traffic intensity measurements of the given road section. A one-minute segment included five personal vehicles and one truck. The results showed that in the given boundary conditions and properties of soil, the stable deformation of the embankment is reached after 324 cycles. The results showed that the deformation of the embankment is only a little higher than the deformation determined in the initial stage and visibly less than the deformation determined when different permanent static loading schemes were applied. The method presented can be suitably used in determining the estimated deformations from a traffic load that can occur under expected or design traffic loading.

REFERENCES

Abdelkrim, M. – Bonnet, G. – de Buhan, P. (2003) *A computational procedure for predicting the long term residual settlement of a platform induced by repeated traffic loading*. Computers and Geotechnics, Vol. 30, No. 6, pp. 463-476. https://doi.org/10.1016/S0266-352X(03)00010-7

Adam, M. - Pflanz, G. – Schmid, G. (2000) *Two- and three-dimensional modelling of half-space and train-track embankment under dynamic loading*. Soil Dynamics and Earthquake Engineering, Vol. 19, pp. 559-573. https://doi.org/10.1016/S0267-7261(00)00068-3

Adamec, J. – Snahnican, J. (2016) *Geotechnické konštrukcie na D1 Hričovské podhradie – Lietavská lúčka (Geotechnical structures on Hričovské podhradie – Lietavská lúčka D1 motorway)*. Engineering geology 2016, 16-17. June, 2016, Vysoke Tatry, Slovakia, pp. 24-31 [in Slovak].

Benz, M. (2007) *Small-strain Stiffness of Soils and Its Numerical Consequences*. Dissertation Thesis. Institute of Geotechnics, University of Stuttgart, 209 pp. Available at: https://www.igs.uni-stuttgart.de/dokumente/Mitteilungen/55_Benz.pdf, (accessed at 03/08/2021).

Dolinajova, K. – Snahnican, J. (2015) *Oporné múry vystužené geomrežami a dvojzákrutovou oceľovou sieťou vystavené vysokému zaťaženiu v seizmickej oblasti (Geogrid and Double Twist Steel Mesh Reinforced Soil Walls Subjected to High Loads in a Seismic Area)*. Proceedings of the 12th Slovak Geotechnical Conference: 55 Years of Geotechnical Engineering in Slovakia, 1-2 June, 2015, Bratislava, Slovakia, pp. 79-87 [in Slovak].

Drusa, M. – Vlcek, J. (2016) *Importance of Results Obtained from Geotechnical Monitoring for Evaluation of Reinforced Soil Structure - Case Study*. Journal of Applied Engineering Sciences, Vol. 6, No. 1, pp. 23-27. https://doi.org/10.1515/jaes-2016-0002

Han, G. – Gong, Q. – Zhou, S. (2015) *Soil Arching in a Piled Embankment under Dynamic Load*. International Journal of Geomechanics, Vol. 15, No. 6, 7 pp. https://doi.org/10.1061/(ASCE)GM.1943-5622.0000443

Holtz, R.D. – Lee, W.F. (2002) *Internal stability analyses of geosynthetic reinforced retaining walls*. Research Report, Agreement No. T9903, Task 95, Geosynthetic Reinforcement III, Washington State Transportation Center, USA, 466 pp. Available at: https://www.wsdot.wa.gov/research/reports/fullreports/532.1.pdf (accessed at 03/08/2021).

Ladicsova, E. (2017) *Deformations of Retaining Structures.* PhD Thesis, Faculty of Civil Engineering, STU in Bratislava, 196 pp [in Slovak].

Liu, P. – Wang, D. – Oeser, M. (2017) *Application of semi-analytical finite element method to analyze asphalt pavement response under heavy traffic loads*. Journal of Traffic and Transportation Engineering (English edition), Vol. 4, No. 2, pp. 206-214. https://doi.org/10.1016/j.jtte.2017.03.003

Mirmoradi, S.H. – Ehrlich, M. (2015) *Modeling of the Compaction-induced Stress on Reinforced Soil Walls*. Geotextiles and Geomembranes, Vol. 43, No. 1, pp. 82-88. https://doi.org/10.1016/j.geotexmem.2014.11.001

Pham, H.V. – Dias, D. (2019) *3D Numerical Modeling of a Piled Embankment under Cyclic Loading*. International Journal of Geomechanics, Vol. 19, No. 4, 15 pp. https://doi.org/10.1061/(ASCE)GM.1943-5622.0001354

PLAXIS 2D CE V21.01:1 (2021) Tutorial Manual. Available at https://communities.bentley.com/products/geotech-analysis/w/plaxis-soilvision-wiki/46137/manuals---plaxis (accessed at 03/08/2021).

Scotland, I. – Dixon, N. – Frost, M. – Wackrow, R. – Fowmes, G. – Horgan, G. (2014) *Measuring Deformation Performance of Geogrid Reinforced Structures Using a Terrestrial Laser Scanner*. Proceedings of 10th International Conference of Geosynthetics, September 2014, Berlin, Germany, 8 pp. Available at: https://www.researchgate.net/publication/286860094_Measuring_deformation_performance_of_geogrid_reinforced_structures_using_a_terrestrial_laser_scanner, (accessed at 03/08/2021).

Scotland, I. – Dixon, N. – Frost, M. – Fowmes, G. – Horgan, G. (2016) *Modelling Deformation During the Construction of Wrapped Geogrid Reinforced Structures*. Geosynthetics International, Vol. 23, No. 3, pp. 219-232. https://doi.org/10.1680/jgein.15.00049

Silber-Hasslacher, T. – Snahnican, J. (2019) *Active and Passive Facing Systems for Reinforced Soil Structures*. 13th Geosynthetics Annual Conference 2019, 7-8 Feb., Zilina, Slovakia, 9 pp. Available at: http://www.geosoul.sk/wp-content/uploads/2019/02/GEOSYNTETIKA2019_ACTIVE-AND-PASSIVE-FACING-SYSTEMS-FOR-REINFORCED-SOIL-STRUCTURES.pdf (accessed at 03/08/2021).

Stacho, J. – Sulovska, M. – Slavik, I. (2020) *Determining the Shear Strength Properties of a Soil-geogrid Interface Using a Large-scale Direct Shear Test Apparatus*. Periodica Polytechnica Civil Engineering, Vol. 64, No. 4, pp. 989-998. https://doi.org/10.3311/PPci.15766

Sulovska, M. – Stacho, J. (2019) *Design of Road Embankment Reinforced Using a Geogrid*. SGEM 2019. 19th International Multidisciplinary Scientific GeoConference. Vol. 19. Science and Technologies in Geology, Exploration and Mining, Sofia, Bulgaria, pp. 145-152. https://doi.org/10.5593/sgem2019/5.4/S22.047

Wang, Z. – Jacobs, F. – Ziegler, M. (2014) *Visualization of Load Transfer Behaviour between Geogrid and Sand Using PFC2D*. Geotextiles and Geomembranes, Vol. 42, No. 1, pp. 83-90. https://doi.org/10.1016/j.geotexmem.2014.01.001

Wu, J.T.H. (1994) *CTI-UCD-1-94: Design and Construction of Low Cost Retaining Walls: The Next Generation in Technology*. Colorado Transport Institute, Denver, Colorado, USA, 1994, p. 152. Available at: https://www.codot.gov/programs/research/pdfs/1994-research-reports/retainingwalls.pdf (accessed at 03/08/2021).

Xuecheng, B. – Hongguang, J. – Yunmin, Ch. (2010) *Accumulative deformation in railway track induced by high-speed traffic loading of the trains*. Earthquake Engineering and Engineering Vibration, Vol. 9, No. 3, pp. 319-326. https://doi.org/10.1007/s11803-010-0016-2

Zheng, L. – Hai-lin, Y. – Wan-ping, W. – Ping, Ch. (2012) *Dynamic stress and deformation of a layered road structure under vehicle traffic loads: Experimental measurements and numerical calculations*. Soil Dynamics and Earthquake Engineering, Vol. 39, pp. 100-112. https://doi.org/10.1016/j.soildyn.2012.03.002

Zhuang, Y. – Li, S. (2015) *Three-dimensional finite element analysis of arching in a piled embankment under traffic loading*. Arabian Journal of Geosciences, Vol. 8, No. 10, pp. 7751–7762. https://doi.org/10.1007/s12517-014-1748-5